Research on the CFD numerical simulation and process optimization of countercurrent–cocurrent dissolved air flotation

Yonglei Wang, Wei Liu, Liping Tian, Ruibao Jia, Zhenqi Du and Anran Zhou

ABSTRACT

The countercurrent–cocurrent dissolved air flotation (CCDAF) process is a new type of air flotation process integrating countercurrent collision and cocurrent flow adhesion processes. The structural form of the CCDAF tank and its process parameters are the required conditions to achieve countercurrent collision and cocurrent adhesion. In this study, eight CCDAF tank process models were established with a flow rate of 0.5 m^3/h. Flow field numerical simulation and process optimization of a CCDAF tank was conducted using Fluent software. The simulation results show that the optimal conditions for the CCDAF process are as follows: contact zone ascending velocity 10 mm/s, separation zone separation velocity 1.5 mm/s, dissolved gas pressure 0.45 MPa, and recirculating dissolved-gas distribution ratio R_1/R_2 1:1. Under these operating conditions, the flow state in the flotation tank is the most stable and the gas in the contact zone is evenly distributed. According to the simulation results, a 5 m^3/h pilot plant was built. The structural dimensions were: $B \times L \times H = 1{,}020\ mm \times 1{,}300\ mm \times 1{,}350\ mm$. The test results show that the CCDAF has a significant decontamination effect and is clearly superior to the cocurrent flow DAF process and countercurrent flow DAF process.

Key words | air flotation, CCDAF, computational fluid dynamics (CFD) numerical simulation, geometry, process parameters

Yonglei Wang (corresponding author)
Wei Liu
Zhenqi Du
Anran Zhou
College of Environmental and Municipal Engineering,
Shandong Jianzhu University,
250101 Jinan,
China
E-mail: *wyl1016@sina.com*

Yonglei Wang
Ruibao Jia
Shandong Province City Water Supply and Drainage Water Quality Monitoring Center,
250021 Jinan,
China

Yonglei Wang
Co-Innovation Center of Green Building,
250101 Jinan,
China

Liping Tian
Weifang Municipal Public Utilities Management Office,
261041 Weifang,
China

INTRODUCTION

In the field of water treatment, dissolved air flotation (DAF) has been widely used in the treatment of high algae micro-polluted water and low-temperature and low-turbidity water (Hu 2013; Zhu *et al.* 2014). The air-floating contact zone is the main place where microbubbles and flocculent particles are mixed, collide, and adhere (Kisner Anderson *et al.* 2016). The operating effect of the air-floating contact zone directly influences the water purification capacity of the DAF process (Lundh *et al.* 2002; Wang *et al.* 2011; Yang *et al.* 2013). The traditional advection DAF process (Figure 1(a)) is essentially a cocurrent flow DAF process. The microbubbles flow in the same direction as the raw water, and the bubbles and flocs have less chance of contact, and the air bubble adhesion effect is not ideal (Albijanic *et al.* 2014). To improve the efficiency of bubble-particle adhesion, a countercurrent DAF process has been developed in recent years (Figure 1(b)). During operation, the microbubbles and the raw water flow in the opposite direction, and the bubbles and the flocs fully collide with each other. However, there are several disadvantages of countercurrent air flotation, such as: low impact load, low efficiency of adhesion of foam flocs, unstable water, and deeper tanks (Guo *et al.* 2002, 2003). To solve the problems of low particle adhesion efficiency, unsatisfactory trapping effect, and unstable adhesion of foam flocs to a single DAF process, countercurrent–cocurrent dissolved air flotation (CCDAF;

doi: 10.2166/aqua.2019.147

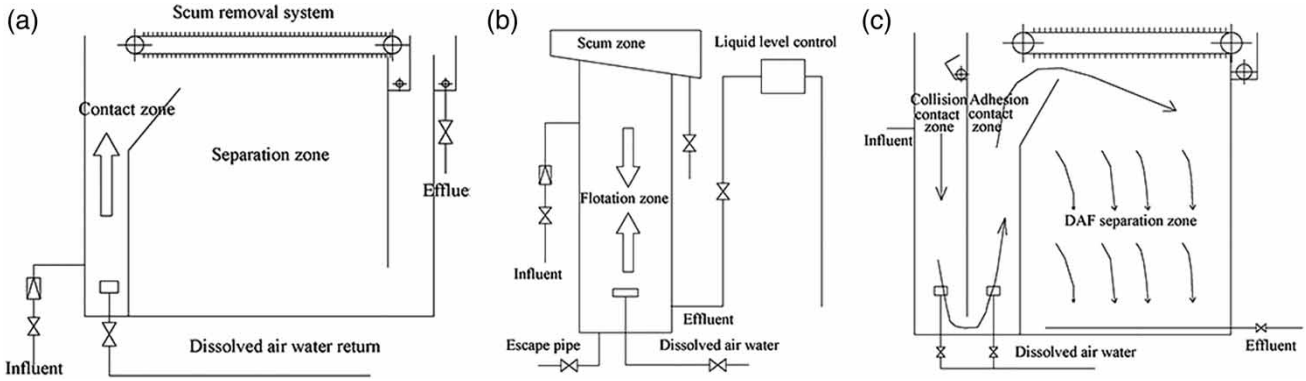

Figure 1 | Sketch of the cocurrent DAF process (a), countercocurrent DAF process (b), and CCDAF process (c).

Figure 1(c)) was developed (Wang *et al.* 2016a, 2016b). This process combines the advantages of cocurrent and countercurrent flow DAF processes. In the CCDAF process, the raw water flows through the collision contact zone and the adhesion contact zone sequentially, which strengthens the adhesion of the microbubbles and enhances the stability of the air-bubble flocs.

The computational fluid dynamics (CFD) method is used to simulate the CFD flow field in the air-flotation tank of the CCDAF process, and the characteristics of the flow field are analyzed to lay a theoretical foundation for the popularization and application of the CCDAF process (Wang *et al.* 2016a, 2016b). The key to the CCDAF tank for countercurrent collision and cocurrent flow adhesion lies in its structure, geometry, and process parameters. At present, the design of the air-floating tank relies on the design manual calculation, and the value is within the parameters given by the specification (Lundh *et al.* 2000a, 2000b). There is no exact method for taking values of parameters, which limits the development of the process (Lundh *et al.* 2002). Based on the previous research, this paper continues to use CFD numerical simulation technology to simulate the flow field of the structure and operation parameters of a CCDAF floating tank. The post-processing patterns such as the gas phase flow pattern and the nephrogram of gas phase volume distribution are used to visually compare the flow patterns in the tank, optimize the geometric dimensions, and process parameters of CCDAF from the perspective of hydraulics, and provide technical support for the popularization and application of CCDAF processes in engineering.

CONSTRUCTION OF THE CCDAF MODEL AND ESTABLISHMENT OF THE CFD NUMERICAL SIMULATION METHOD

CCDAF test device

The CCDAF process is a new type of air floatation process that incorporates countercurrent collision and co-current adhesion processes. The air flotation tank of the CCDAF process includes a countercurrent collision contact zone, a cocurrent adhering contact zone, and an air flotation separation zone. The difference between the CCDAF and the traditional DAF process is that the air-floating contact zone is divided into two stages, namely, a collision contact zone and an adhesion contact zone. Gas-dissolved water is added twice. In the collision contact zone, the microbubbles and raw water countercurrently flow, achieving full collision of the microbubbles with the suspended matter, which become larger with flocculation. The air-bubble flocs then enter the adhesive contact zone as the effluent of the collision contact zone. In the adhesive contact zone, the microbubbles flow in the same direction as the raw water and come into contact. Some of the microbubbles in the collision contact zone enter the adherent contact zone with the water flow. This process increases the concentration of the microbubbles in the adhesion contact zone and also enhances the adhesion of the microbubbles to the suspended matter. Finally, air-bubble flocs are formed and float to the separation zone.

The air flotation tank diagram is shown in Figure 2(a). To facilitate the CFD numerical simulation of the CCDAF process, the CCDAF tank boundary conditions and tank body

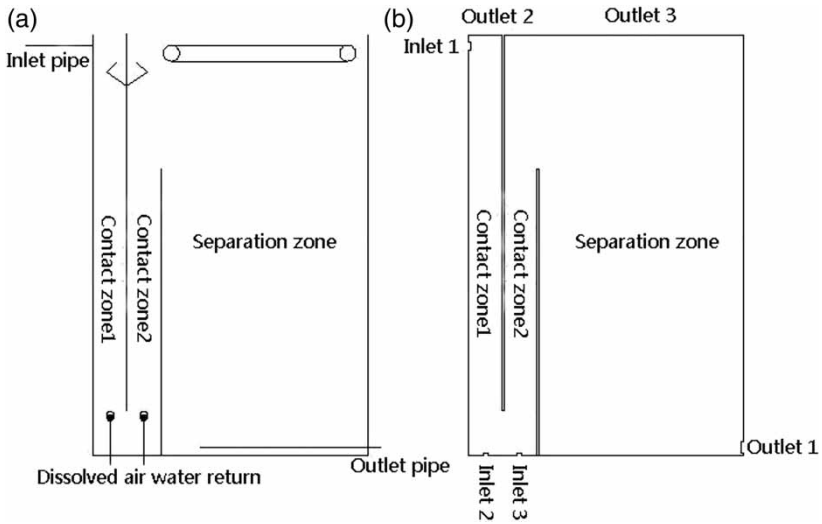

Figure 2 | Sketch of the air flotation tank (a) and model (b).

are simplified. The simplified model is shown in Figure 2(b). The raw water enters contact zone 1 from inlet 1 and the gas-dissolved water flows back to the contact zone through inlet 2 and inlet 3. The recycle ratios of contact zone 1 and contact zone 2 are R_1 and R_2, respectively.

Process model design and grid building

According to the preliminary parameter optimization test, the total recycle ratio ($R_1 + R_2$) is 10%, and design flow rate is 0.5 m^3/h. According to the design manual recommendation, we calculated all the models of 16 size types with the contact zone rising velocity of 10–25 mm/s and the separation zone separation velocity of 1.5–2.5 mm/s. Further screening was carried out according to the design specifications, and the models' contact times less than 60 s were excluded, and finally eight models meeting the specification requirements were obtained. The model parameters are shown in Table 1.

Before using Fluent 14.5 for calculations, we needed to use pre-processing software to build the grid (Kaminsky *et al.* 2005). The study used ICEM CFD 14.5 for pre-processing and a two-dimensional bilinear over-limit difference method to create a structured grid (Pashchenko 2018). The established mesh model is shown in Figure 3. The number of grids is the same as in Table 1.

All of the above grid determinant quality detection values are 1; Angle quality detection values are all 90, indicating that all grids have an angle of 90° and the grid quality is excellent.

Table 1 | List of the model parameters

Model number	Rising velocity of contact zone (mm/s)	Separation velocity of separation zone (mm/s)	Length (mm)	Height (mm)	Number of grids
a	10	1.5	1,300	1,350	69,392
b	10	2.0	1,050	1,800	74,432
c	15	2.0	1,430	1,800	101,432
d	20	2.0	1,800	1,800	128,432
e	10	2.5	900	2,250	79,472
f	15	2.5	1,200	2,250	106,784
g	20	2.5	1,500	2,250	133,472
h	25	2.5	1,800	2,250	160,534

Control equation

This test does not involve heat transfer and assumes that liquid water is not compressible. Therefore, Fluent only needs to solve the continuity equation, the energy equation, and the momentum equation.

Continuity equation

The differential form of the continuity equation can be expressed as:

$$\frac{\partial \rho}{\partial t} + \frac{\partial}{\partial x_i}(\rho u_i) = S_m \tag{1}$$

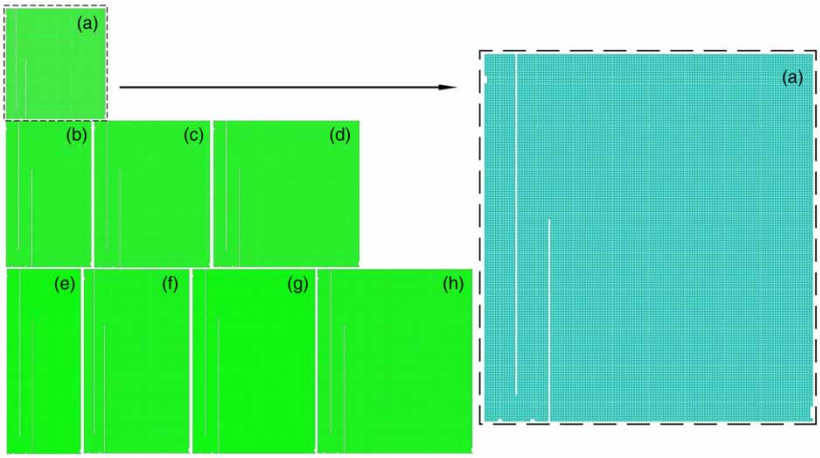

Figure 3 | Physical models of eight air flotation tanks, meshes (a)–(h) and a magnified view of the model (a).

This equation applies to both compressible and incompressible flows. S_m is the source item.

Momentum equation

In the inertial coordinate system, the momentum conservation equation in direction-i can be expressed as:

$$\frac{\partial}{\partial t}(\rho u_i) + \frac{\partial}{\partial x_j}(\rho u_i u_j) = -\frac{\partial p}{\partial x_i} + \frac{\partial \tau_{ij}}{\partial x_j} + \rho g_i + F_i \quad (2)$$

τ_{ij} is stress tensor, its expression is $\tau_{ij} = \left[\mu\left(\frac{\partial u_i}{\partial x_j} + \frac{\partial u_j}{\partial x_i}\right)\right] - \frac{2}{3}\mu\frac{\partial u_l}{\partial x_l}\delta_{ij}$, p is static pressure, g_i and F_i are the gravitational volume force and the external volume force in the i directions.

Energy equation

The energy equations solved by Fluent are as follows:

$$\frac{\partial}{\partial t}(\rho E) + \frac{\partial}{\partial x_i}[u_i(\rho E + p)] = -\frac{\partial}{\partial x_i}\left(k_{eff}\frac{\partial T}{\partial x_i}\right) - \sum_{j'} h_{j'} J_{j'} + u_j(\tau_{ij})_{eff} + S_h \quad (3)$$

$$E = h - \frac{p}{\rho} + \frac{u_i^2}{2}$$

In Equation (3), k_{eff} is the effective heat transfer coefficient, J_j is the diffusion flow of component j, S_h is the heat of reaction. Other parameters have the same meaning as above.

CFD numerical simulation method and boundary condition

Fluent 14.5 (Ansys Inc., USA) is the most widely used CFD software (Ye *et al.* 2006). Fluent offers three multiphase flow models, the Volume of Fluid model, the Mixture model, and the Eulerian model (Kaminsky *et al.* 2005; Hu 2010; Yu *et al.* 2011). The mixture model is a simplified multiphase flow model. It is mainly used to simulate two-phase or multiphase flow. The multiphase flow can be either a fluid or a particle (Han *et al.* 2011). This experiment mainly studies the characteristics of the flow field in the air flotation tank. The core of the experiment is the status of microbubbles in the flow field, including the movement of microbubbles and the distribution of microbubbles (Chao *et al.* 2011; Wei & Song 2015; Alizadeh & Khamehchi 2016). The flow in the air flotation tank is turbulent, so the turbulence model adopts the k-ε viscosity model.

The model boundary settings are shown in Figure 4. The water inlet to be treated is set to IN1, the two reflux dissolved water inlets are set to IN2 and IN3, the treated water outlet is set to OUT1, the two tank top free surfaces are set to OUT2, OUT3, and finally, the tank wall is set to WALL. According to the preliminary parameter optimization test, the inflow flow rate is 0.5 m^3/h, the recycle ratio is 10%, the inlet pipe diameter is 32 mm, the outlet pipe diameter is 50 mm, and the reflux dissolved water inlet pipe diameter is 20 mm. Except for the top free surfaces OUT2 and OUT3, which are defined as pressure outlets, the

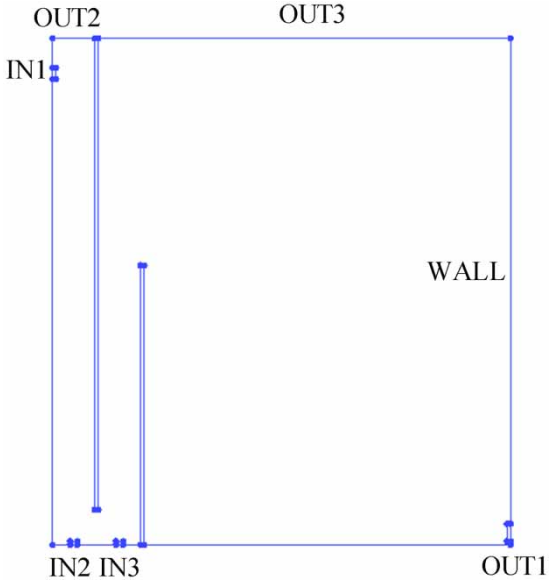

Figure 4 | Air flotation tank boundary settings.

others are velocity inlets. According to the air/water flow ratio measured by the experiment, the reflux inlet bubble volume fraction was set to 0.0479. Average bubble diameter is 40–50 μm. The WALL uses no sliding wall conditions. The free surface at the top is the water surface, and the simulation is set to the symmetry boundary condition, ensuring that there is no vertical velocity component at the surface and the wall friction is zero. In addition, the UDF (user define function) is applied to the adjacent grid on the surface to increase the quality source term and describe the bubble overflow process. Calculations of the parameters of each velocity entry boundary condition according to the above conditions are shown in Table 2.

Table 2 | Each speed entry boundary condition parameter

Boundary	Type	Velocity v (m/s)	Hydraulic diameter D_H (mm)	Turbulence intensity I (%)
IN1	Velocity-inlet	0.173	32	5.45
IN2	Velocity-inlet	0.022	20	7.48
IN3	Velocity-inlet	0.022	20	7.48
OUT1	Velocity-inlet	−0.078	50	5.70

FLOW FIELD SIMULATION AND PROCESS OPTIMIZATION OF THE CCDAF AIR FLOTATION TANK MODEL

Geometry optimization

Analysis of pathlines of gas-phase velocity

The pathlines of gas-phase velocity (Figure 5) show the flow path of gas in gas-dissolved water. In models (a), (b), and (h), the microbubble particle passes through the countercurrent collision zone, cocurrent flow contact zone, and air flotation separation zone in sequence and that trajectory of the model particles is basically the same. Most of the dissolved water entering from inlet 2 enters contact zone 1, the trajectory of the gas-liquid flow point is obvious, and the reverse impact contact effect between bubble and floc is significant. The overall flow state in the air flotation tank is good, and the velocity of the water flow in the contact area is large, while the flow velocity of water in the separation area is significantly reduced and the flow state is stable, which can reduce the fragmentation and desorption of the air-bubble flocs. A favorable environment is formed in these models to facilitate the collision and adhesion of microbubble and flocs, and it is also conducive to the removal of air-bubble flocs. In the models (c), (d), (e), (f), and (g), the dissolved gas water entering from water inlet 2 is mostly influenced by the water flow and enters contact zone 2, and the amount of gas entering contact zone 1 is relatively small, which results in a non-obvious gas-phase flow in contact zone 1 and a relatively weak contact effect between the microbubbles and flocs. In addition, the flow velocity in the separation zone did not decrease significantly, which was not conducive to the floc floating separation.

In the eight models, the flow velocity of the gas-liquid particles at the right baffle of contact zone 2 was fast. After entering the separation zone, the gas is affected by the flow of water in the descending process and there are different degrees of reflux phenomena, and both return to the inlet. The turbulence, backspin, and vortex phenomena of models (e), (f), and (h) are significant and can easily disturb the formed air-bubble flocs and cause them to break as well as affect their adhesion stability, which is detrimental to the air flotation effect. The stability of the flow field in the

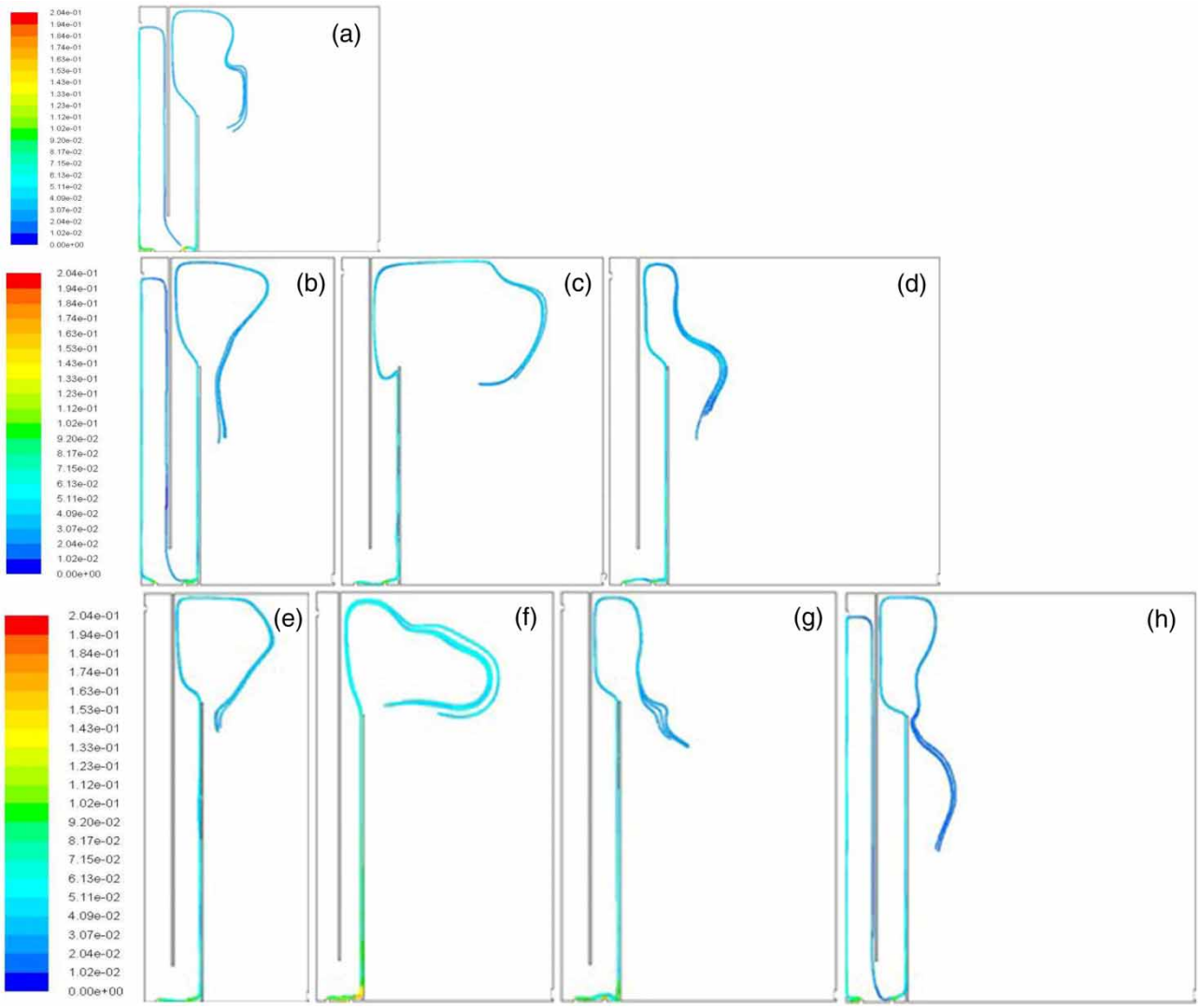

Figure 5 | Pathlines of gas-phase velocity of eight models in the CCDAF tank (a)–(h).

separation zone is conducive to stable adhesion of the air-bubble flocs, and the desorption phenomenon is less likely to occur. The trajectories of the gas-phase flow lines in models (a), (b), and (c) are smooth and difficult to generate perturbations for, which is beneficial to the floating and removal of the air-bubble flocs.

Based on the above analysis of the characteristics of the gas flow streamlines in the contact zone and the separation zone, we observe that: models (a) and (b) can realize the reverse collision of foam floccules and co-directional adhesion and stable adhesion of the separation zone, which is a more appropriate process size model.

Contour of bubble concentration analysis

The contour of bubble concentration represents the volume occupied by the gas phase at different positions in the air-flotation tank, and can more directly to indicate the gas-phase volume of fraction at different positions. The contour of bubble concentration of each model is shown in Figure 6.

From Figure 6, it is observed that contact zone 1, contact zone 2, and the separation zone of the CCDAF flotation tank are covered with microbubbles. The number of micro-bubbles in the contact zone is large, and the bubble

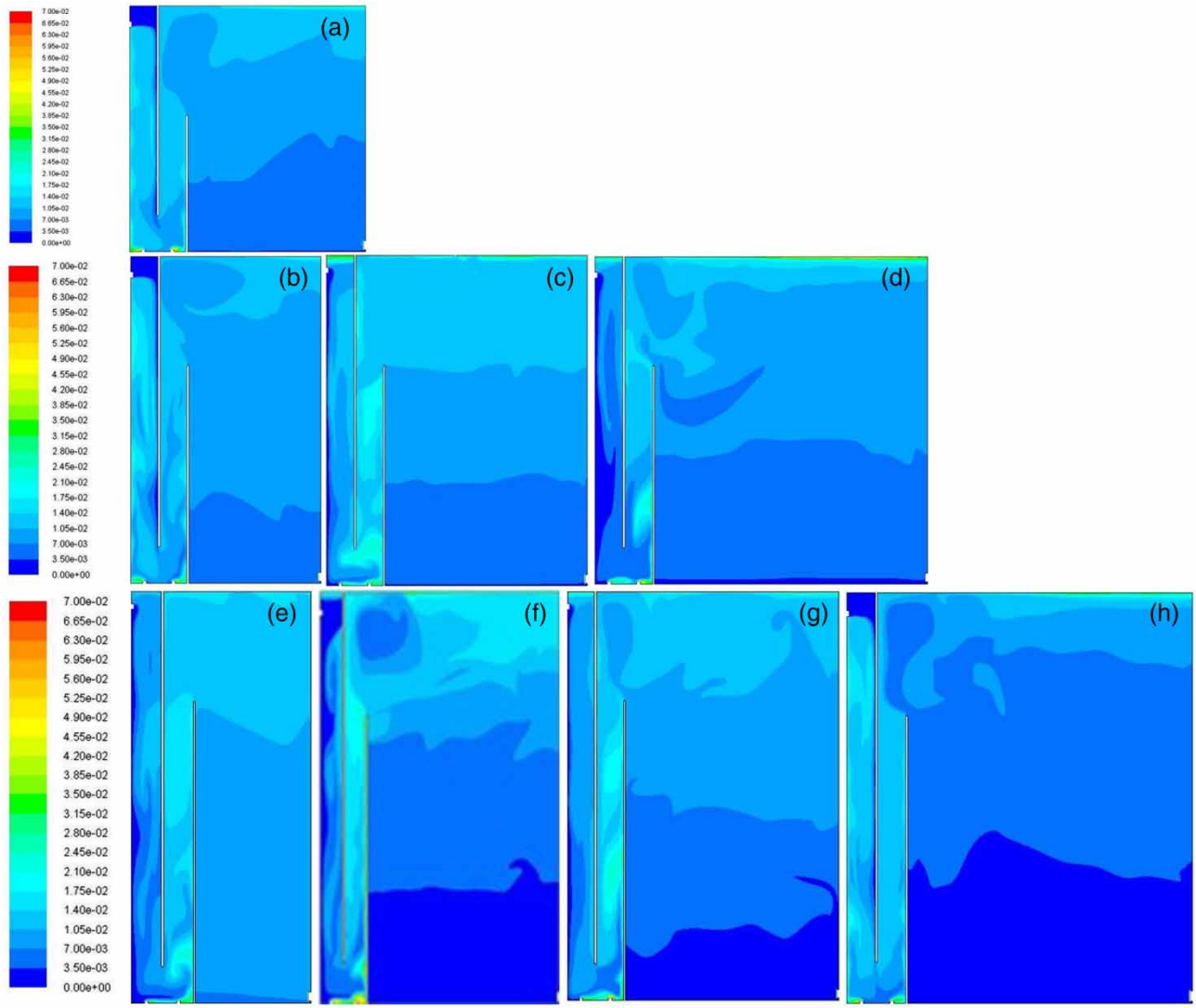

Figure 6 | Contour of bubble concentration of eight models (a)–(h).

concentration in contact zone 2 is higher than that in contact zone 1. The microbubbles gather in the upper part of the separation zone. The degree of disturbance and distribution of microbubbles in each area are influenced by the geometric size of the flotation tank and the flow velocity, and there are large differences.

The gas-phase distributions of contact zone 1 and contact zone 2 in the air-flotation models (a) and (h) are relatively uniform, the flow state is stable, and there are no adverse turbulences, such as an obvious backflow. In models (b), (c), (d), (e), (f), and (g), the gas flow distributions in contact zone 1 and contact zone 2 are not uniform and the disturbance is significant. In addition, the gas phase volume in contact zone 1 in the models (c), (d), (e), (f), and (g) is relatively low, which is not conducive to the collision of microbubbles and flocs. In the separation zone, the distribution of microbubbles in models (a), (c), and (e) is relatively uniform, which facilitates the flotation of the air-bubble flocs in a stable flow state and removal. The air bubbles in the upper part of the separation zone have a high concentration, and a thick layer of microbubbles is gathered. The microbubbles gradually decrease in concentration from the top to bottom and gradually decrease along the depth of the tank. The microbubble layer has a

good filtering function. Models (b), (d), (f), (g), and (h) all have different degrees of non-uniform gas-phase distributions, and there is turbulence or a vortex at the inlet of the separation zone, which creates disturbances and easily causes the formed air-bubble flocs to break.

According to the contour of bubble concentration, the model (a) gas distribution in the contact zone is uniform, the flow state is stable, the gas distribution in the separation zone is stepped and evenly distributed, there is no obvious backflow, and the gas-phase distribution is reasonable. Therefore, model (a) is the recommended model for the CCDAF tank design.

Through a comprehensive analysis of the pathlines of gas-phase velocity of each model and the contour of bubble concentration, model (a) is determined to be the best model. The size parameters are: $B \times L \times H = 102\ mm \times 1{,}300\ mm \times 1{,}350\ mm$. The ascending flow rate in the contact zone is 10 mm/s, and the separation zone separation velocity is 1.5 mm/s.

Process parameter optimization

Dissolved air pressure optimization

The dissolved air pressure and gas-dissolved water recirculation ratio are two important parameters in the operation process of a CCDAF air flotation tank, and the magnitude of its value directly affects the operation effect of the process. The dissolved gas pressure directly affects the gas holdup of the dissolved water, thereby affecting the size and distribution of the microbubbles in the flotation tank. During the experiment, the dissolved gas pressure is maintained at 0.30–0.50 MPa. According to the magnitude of the outgas volume of the dissolved gas device under different pressure conditions, the corresponding gas holdup is shown in Table 3. Taking model (a) as the simulation object, five different gas holdup conditions were selected for simulation. Boundary condition settings are: inlet 1 influent flow is 0.5 m^3/h, inlet velocity is 173 mm/s, recycle ratio is 10%; inlet 2 and inlet 3 inlet velocity are 22 mm/s, and average bubble diameter is 40–50 μm. The gas holdups are 2.4%, 4.5%, 6%, 6.8%, and 7.5%, which correspond to the dissolved-air pressures of 0.3 MPa, 0.35 MPa, 0.4 MPa, 0.45 MPa, and 0.45 MPa, respectively. The distribution of microbubbles in the flotation tank at different pressures of dissolved gas are shown in Figure 7.

Table 3 | Corresponding table of dissolved gas pressure and gas holdup

Dissolved gas pressure (MPa)	0.3	0.35	0.4	0.45	0.5
Air precipitating amount (mL)	24	45	60	68	75
Gas holdup (%)	2.4	4.5	6.0	6.8	7.5

Figure 7 shows that when the pressure is less than 0.45 MPa, most of the microbubbles in inlets 2 and 3 flow to contact zone 2 under the action of the water flow. As a result, the distribution of the microbubbles in contact zone 1 and contact zone 2 is not uniform. Especially, in contact zone 2, the disturbance of the gas flow is large, resulting in poor contact between the microbubbles and flocs. At the same time, the distribution of the microbubble layer in the air flotation separation zone is also very uneven, which is not conducive to the stable flotation of the air-bubble flocs. When the pressure reaches 0.45 MPa and above, the gas-dissolved water at water inlet 2 rises into contact zone 1 along the wall of the inlet side under pressure and contact zone 1 is filled with a uniform microbubble layer, achieving a collision of bubbles and flocs. In addition, the gas-phase distribution in the air-floating contact zone and separation zone is relatively uniform, which is conducive to the collision of microbubbles as well as the stable flotation of the air-bubble flocs. Therefore, the CCDAF flotation tank is recommended to have a dissolved air pressure of 0.45 MPa.

Optimization of two recycled flows to two contact zones ratio (R_1:R_2)

Under the condition of a dissolved gas pressure of 0.45 MPa, the dissolved water distribution ratio of model (a) was optimized to simulate the gas-phase flow regime in the CCDAF tank under different distribution ratios. The gas phase volume distribution cloud diagrams at different distribution ratios are shown in Figure 8.

It is observed from Figure 8 that when the distribution ratio R_1:R_2 is small, most of the gas-dissolved water entering from water inlet 2 flows horizontally into contact zone 2 under the action of the water flow. The number of microbubbles in contact zone 2 is significantly more than that in contact zone 1. However, the distribution of microbubbles

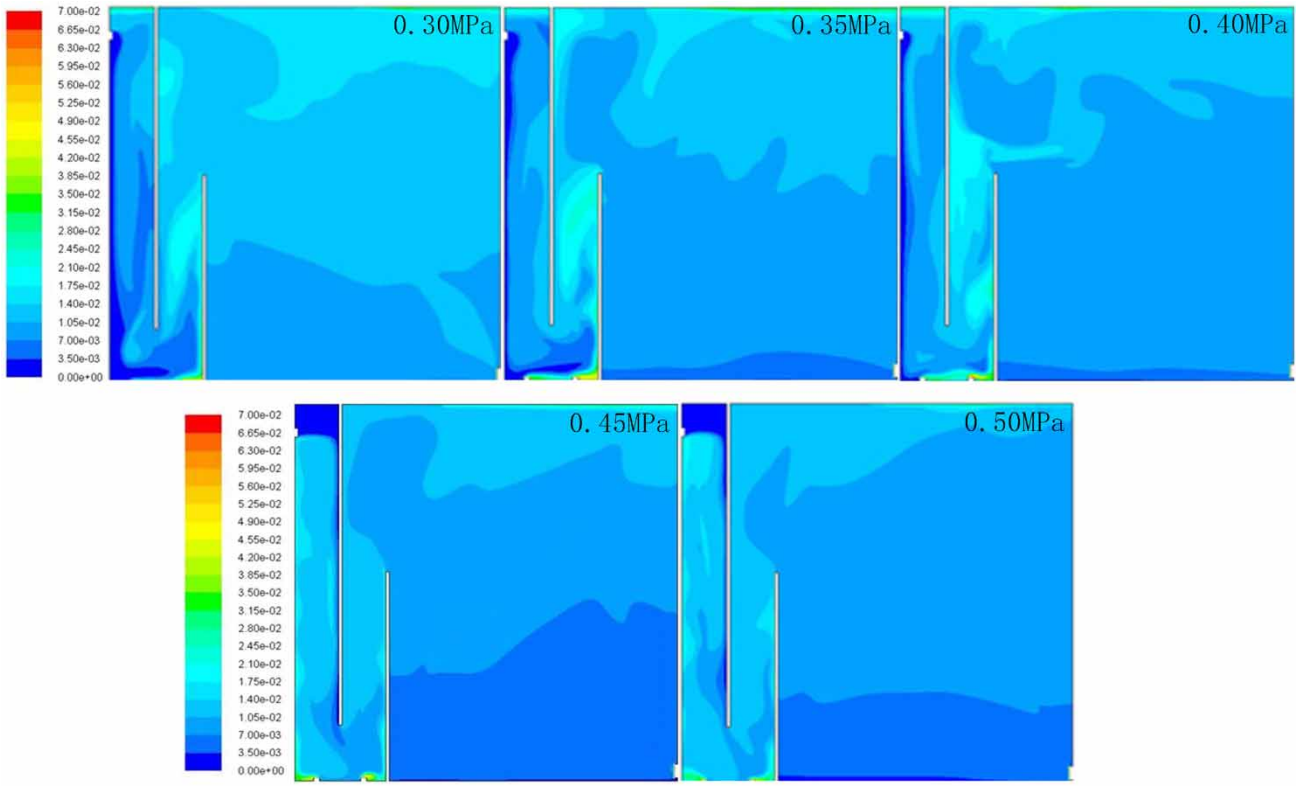

Figure 7 | Contour of bubble fraction in CCDAF tank under different pressures of dissolved gas (0.30–0.50 MPa).

in contact zone 2 is not uniform. Due to the small number of microbubbles in contact zone 1, the reverse impact contact effect is weak. As observed from Figure 8, when R_1:R_2 is 1:5, two vortex areas appear at the inlet end of the separation zone. This phenomenon has a destructive effect on the formed air-bubble flocs. When R_1:R_2 reaches 1:1, the concentration of microbubbles in contact zone 1 and contact zone 2 is basically the same and the distribution is even. The gas-dissolved water entering through water inlet 2 rises near the inlet side wall. Under the action of the water flow, the water to be treated is thoroughly mixed and contacted and then flows down together into contact zone 2. When R_1:R_2 is 2:1 or 3:1, the concentration of microbubbles in contact zone 1 is greater than that in contact zone 2. There is a certain disturbance in the flow state in the separation zone, which increases with the increase of the distribution ratio. At the same time, due to the accumulation of a large number of microbubbles in contact zone 1, the gas phase distribution volume in the separation zone gradually decreases. When R_1:R_2 reaches 4:1 or more, the flow state in the air-floating contact zone 1 and contact zone 2 is complicated and the turbulent flow is intensified, which is not favorable for the adhesion of air-bubble flocs. In summary, it is more appropriate to control the dissolved water distribution ratio to be approximately 1:1.

CONTRAST TEST OF DECONTAMINATION PERFORMANCE OF CCDAF PILOT PLANT

According to the CFD simulation and optimization results, a 5 m^3/h CCDAF pilot plant was established. We performed similar CFD numerical simulation and parameter optimization experiments on a cocurrent DAF tank and countercocurrent DAF tank under the same conditions. The respective optimal model dimensions and operating parameters were obtained, and the corresponding pilot plant was established. Since the flow rate of the pilot plant is 5 m^3/h, it is ten times the model design flow. Thus, we keep the length and height unchanged, and expand the

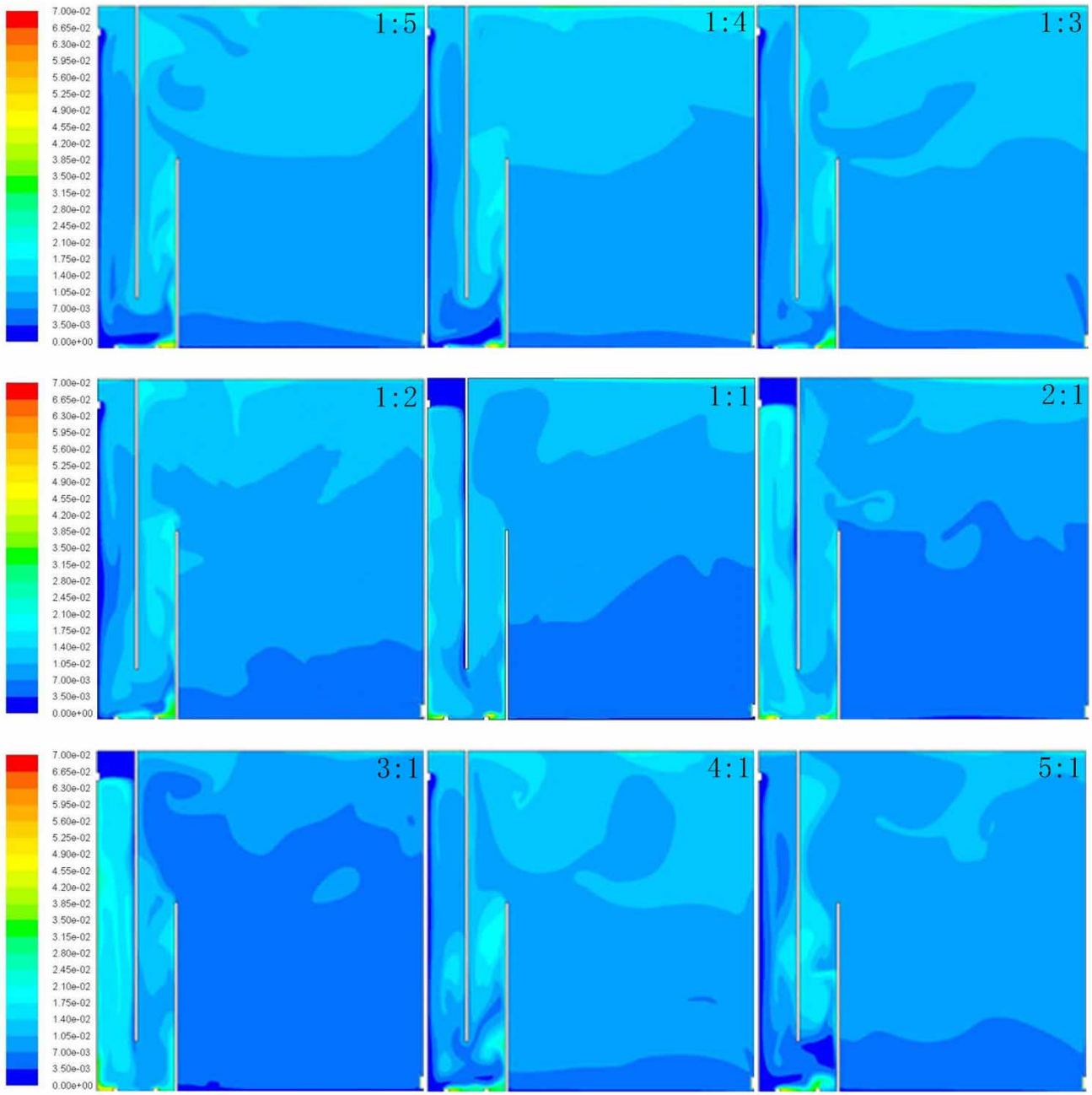

Figure 8 | Contour of bubble fraction of different distribution ratios of reflux gas-dissolved water at the inlet (1:5–5:1).

width by ten times. Equipment parameters are shown in Table 4. The dissolved gas pressure, recycle ratio, and R1: R2 are consistent with the simulation results, ensuring that rising velocity of the contact zone and separation velocity of the separation zone does not change. The bubble size depends on the dissolved gas pressure and does not change with dimensional changes.

Three pilot plants were stably operated for 20 days under the same coagulation conditions, and the effluent from each flotation tank was taken every day for indicator detection. The 20-day average removal rate of pollutants from different processes is shown in Figure 9.

As observed from Figure 9, the CCDAF process has a better decontamination efficiency than the cocurrent and

Table 4 | Pilot equipment size and parameters

Air float type	CCDAF	Cocurrent DAF	Countercurrent DAF
Device size B × L × H (mm)	1,020 × 1,300 × 1,350	680 × 1,430 × 1,800	510 × 1,500 × 2,250
Contact zone length (mm)	150	150	150
Separation zone length (mm)	1,000	1,130	1,200
Pressures of dissolved gas (Mpa)	0.45	0.45	0.40
Recycle ratio	10%	10%	10%
R_1:R_2	1:1		

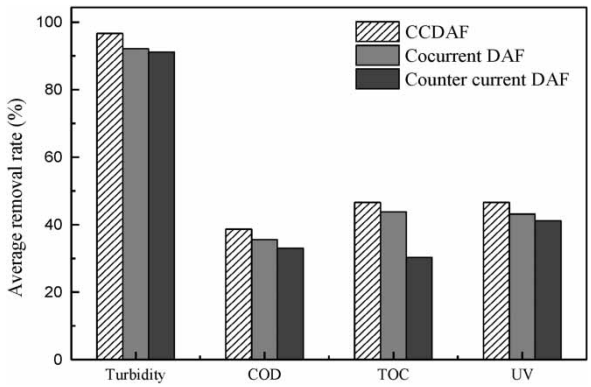

Figure 9 | Comparison of removal effects of different processes under optimal conditions.

countercurrent DAF processes. In terms of turbidity removal, the removal rate of the CCDAF process is 4.53% and 5.56% higher than those of the cocurrent and countercurrent DAF processes, respectively. The removal rate of organic matter is basically the same as the removal of turbidity; CCDAF has the best effect, followed by the cocurrent DAF, and the countercurrent DAF is the worst. Compared with the cocurrent DAF processes, the removal effects of CCDAF on COD_{Mn}, TOC, and UV_{254} were improved by 3.13%%, 2.84%, and 3.49%, respectively. Compared to countercurrent DAF processes, the removal effects of CCDAF on COD_{Mn}, TOC, and UV_{254} increased by 5.67%, 16.34%, and 5.52%, respectively. The excellent decontamination performance of CCDAF benefits from the interaction of the countercurrent collision contact zone and the cocurrent adhesion contact zone. This improvement increases the contact and adhesion efficiency of the microbubbles with the flocs, and forms air-bubble flocs which are easier to separate, so that the effluent water quality is better than the cocurrent DAF tank and countercocurrent DAF tank. We recommend the use of CCDAF when conditions permit.

CONCLUSION

Simulation of the flow field and parameter optimization of eight CCDAF tank models were performed. The results show that the water flow in the CCDAF tank is good overall, that the flow state is stable, and that it can realize reverse collision of air-bubble flocs and adhere in the same direction. At a flow rate of 0.5 m^3/h, the optimal tank configuration parameters for the CCDAF tank are as follows: B × L × H = 102 mm × 1,300 mm × 1,350 mm; the ascending flow rate in the contact zone is 10 mm/s; the separation velocity of the separation zone is 1.5 mm/s. When the dissolved gas pressure is 0.45 MPa and the R_1:R_2 ratio is approximately 1:1, the gas in the contact zone is evenly distributed. The gas distribution in the separation zone is evenly distributed in a step-like manner. There is no obvious backflow, and the gas phase distribution is reasonable.

Using the simulation and optimization results of three air flotation processes, a 5 m^3/h pilot test device was established. The structural dimensions were: B × L × H = 1,020 mm × 1,300 mm × 1,350 mm. The test results show that the CCDAF has a significant pollution removal effect and is obviously superior to the cocurrent DAF processes and countercurrent DAF processes. Compared with the cocurrent DAF processes, the removal effects of CCDAF on turbidity, COD_{Mn}, TOC, and UV_{254} were improved by 4.53%, 3.13%, 2.84%, and 3.49%, respectively. Compared with countercurrent DAF processes, the removal effects of

CCDAF on turbidity, COD_{Mn}, TOC, and UV_{254} increased by 5.56%, 5.67%, 16.34%, and 5.52%, respectively.

ACKNOWLEDGEMENTS

This work was financially supported by the Natural Science Foundation of Shandong Province (ZR2016EEM32), Science and Technology Plans of Ministry of Housing and Urban-Rural Development of the People's Republic of China, and Opening Projects of Beijing Advanced Innovation Center for Future Urban Design, Beijing University of Civil Engineering and Architecture (Research and application of key technologies for dissolved air flotation based on water purification of algae-contaminated lakes, UDC2017031612), and the Doctoral Fund of Shandong Jianzhu University in 2015 (XNBS1511).

REFERENCES

Albijanic, B., Ozdemir, O., Hampton, M. A., Nguyen, P. T., Nguyen, A. V. & Bradshaw, D. 2014 Fundamental aspects of bubble–particle attachment mechanism in flotation separation. *Minerals Engineering* **65**, 187–195.

Alizadeh, A. & Khamehchi, E. 2016 Stability modeling of water-based surfactant covered micro-bubble fluids. *Journal of Surfactants & Detergents* **19**, 165–171.

Chao, Z., Wang, Y., Jakobsen, J. P., Fernandino, M. & Jakobsen, H. A. 2011 Derivation and validation of a binary multi-fluid Eulerian model for fluidized beds. *Chemical Engineering Science* **66**, 3605–3616.

Guo, J. L., Wang, Y. L., Da-Peng, L. I. & Tang, H. X. 2002 Counter current co-flocculation flotation-new water treatment method. *China Water & Wastewater* **18**, 12–16.

Guo, J. L., Wang, Y. L., Da-Peng, L. I. & Tang, H. X. 2003 Counterflow co-flocculation flotation for water purification. *Journal of Environmental Science and Health, Part A* **38**, 923–934.

Han, K., Liu, A., Peng, D., Sun, D. & Wang, J. 2011 Numerical simulation of flow boiling heat transfer in sintered surface porous tubing. *Chemical Engineering & Machinery* **1**, 547–552.

Hu, W. 2010 Simulation of flow around multi-circular-cylinders based on Fluent. *Science & Technology Review* **28**, 75–78.

Hu, H. 2013 *Enhanced Coagulation of Yellow River Water at Low Temperature and Turbidity*. Master's thesis, Zhengzhou University, China.

Kaminsky, J., Rodt, T. & Gharabaghi, A. 2005 A universal algorithm for an improved finite element mesh generation mesh quality assessment in comparison to former automated mesh-generators and an analytic model. *Medical Engineering & Physics* **27**, 383–394.

Kisner Anderson, M., Penalva Reali, M. A. & Pioltine, A. 2016 Evaluation of the effects of varying the water velocity at the entrance of the contact zone on the performance of a dissolved air flotation (DAF) unit using the image analysis method. *Water Science & Technology: Water Supply* **16**, 802–809.

Lundh, M., Jönsson, L. & Dahlquist, J. 2000a Experimental studies of the fluid dynamics in the separation zone in dissolved air flotation. *Water Research* **34**, 21–30.

Lundh, M., Jönsson, L. & Dahlquist, J. 2000b The flow structure in the separation zone of a DAF pilot plant and the relation with bubble concentration. *Water Science and Technology* **43** (8), 185–194.

Lundh, M., Jönsson, L. & Dahlquist, J. 2002 The influence of contact zone configuration on the flow structure in a dissolved air flotation pilot plant. *Water Research* **36**, 1585–1595.

Pashchenko, D. I. 2018 Ansys Fluent CFD modeling of solar air-heater thermoaerodynamics. *Applied Solar Energy* **54**, 32–39.

Wang, Y., Wang, Q., Zhuo, S. & Li, N. 2011 Improvement of operational mode of counter-current dissolved air flotation process. In: *International Conference on Digital Manufacturing and Automation, 2011*. IEEE, pp. 838–841.

Wang, M., Zhang, K., Li, J. & Wang, Y. 2016a Application of computational fluid dynamics in the design of flotation tank. *Water & Wastewater Engineering* **S1**, 297–301.

Wang, Y. L., Liu, B. Z., Zhang, K. F., Li, M., Jia, R. B., Song, W. C. & Li, J. 2016b Construction and operation characteristics of countercurrent-cocurrent dissolved air flotation (CCDAF). *CIESC Journal* **67**, 5252–5258.

Wei, H. P. & Song, F. U. 2015 Multiphase models for flow field numerical simulation of a vehicle rising from water. *Journal of Vibration and Shock* **34** (4), 48–52.

Yang, R. Q., Wang, H. F. & Liu, J. C. 2013 Jet flotation column system structure design and numerical simulation of two-phase flow. *Advanced Materials Research* **616–618**, 655–661.

Ye, X., Wang, X. & Bi, L. 2006 The numerical simulation of SK static mixer according to the CFD software Fluent. *Modern Manufacturing Engineering* **3**, 74–75.

Yu, Y., Fan, Y., Xu, G. L. & Wang, Q. 2011 Hydraulic simulation of MBR with computational fluid dynamics. *Membrane Science and Technology* **31**, 9–16.

Zhu, I. X., Bates, B. J. & Anderson, D. M. 2014 Removal of Prorocentrum minimum from seawater using dissolved air flotation. *Journal of Applied Water Engineering and Research* **2**, 47–56.

First received 14 November 2018; accepted in revised form 13 April 2019. Available online 31 May 2019